Int. J. Advanced Design and Manufacturing Technology, 2024, Vol. 17, No. 2, pp. 1-6

DOI: 10.30486/ADMT.2024./873443 *ISSN: 2252-0406* *https://admt.isfahan.iau.ir*

Numerical Analysis of Fluid-Structure Interaction in The Aortic Arch Considering Various Blood Flow Rates

Hamid Zandvakili, Kamran Hassani*, Siamak Khorramymehr

Department of Biomedical Engineering, College of Medical Science and Technologies, Tehran Science and Research Branch, Islamic Azad University, Tehran, Iran

E-mail: dr.zandvakili@gmail.com, k.hasani@srbiau.ac.ir, s.khorramymehr@srbiau.ac.ir

*Corresponding author

Received: 7 February 2023, Revised: 26 July 2023, Accepted: 10 April 2023

Abstract: Hemodynamic forces are felt by the biomechanical receptors of the arterial wall to give an appropriate response to maintain homeostasis. On the other hand, baroreceptors are a type of biomechanical receptors that are sensitive to abnormal stretch sizes. It is very important to predict the distribution of stress and strain caused by the hemodynamic field to the vessel wall in pressure-sensitive areas to evaluate the function of these receptors. In the present study, a three-dimensional (3-D) model of the aortic arch is presented. The geometry was reconstructed based on the CT images. Also, numerical analysis was performed using the fluid-structure interaction method. First, the hemodynamic field containing the pressure and velocity distribution in the blood area was obtained. Then, the deformation and stress fields in the solid domain were analyzed. The results show that the highest vertical stress occurs in the posterior supra aorta. So, the amount of this maximum vertical stress increases up to 5 kPa in some places; these points have higher tensions, and they can be susceptible to rupture and aneurysm diseases. Higher normal stress happened at the aortic root and the supra-aortic branches and reached approximately 200 kPa at Peak Systole. Also, the highest amount of strain occurs in the posterior supra aorta, reaching 0.001.

Keywords: Aortic Arch, FSI Method, Hemodynamics, Numerical Modeling, Perfusion

Biographical notes: Hamid Zandvakili received his BSc in Mechanical Engineering from Shahid Bahonar University of Kerman. He received his MSc in biomechanics from the Science and Research Branch of Islamic Azad University and is currently a PhD candidate in biomechanical and biomedical engineering at this university. **Kamran Hassani** received his PhD in biomedical engineering from Amirkabir University. He is currently an associate professor at the Science and Research Branch of Islamic Azad University. His field of research is mainly cardiovascular system biomechanics. **Siamak Khorramymehr** received his PhD in biomedical engineering from the Science and Research Branch of Islamic Azad University. He is currently an Assistant Professor in Medical Sciences and Technologies at the Science and Research Branch of Islamic Azad University. His field of research is mainly biomechanics, ergonomics, and rehabilitation engineering.

Research paper

1 INTRODUCTION

Cardiovascular diseases are one of the common diseases in today's societies that can be caused by problems in the blood vessels and the behavior of the blood in the veins. In order to recognize these diseases, there must be enough information about the behavior of the blood, such as changes in blood pressure and velocity profiles, as well as changes in tension and changes in the shape of the walls of the vessels. On the other hand, the baroreflex is a homeostasis mechanism of the body that is used to keep blood pressure constant. This reflex is involuntary and is considered a quick self-regulation. The baroreceptor system plays an important role in the short-term regulation of blood pressure, which is mediated by baroreceptors. These receptors are located in the carotid arteries, the aortic arch, and the walls of the heart cavities and are activated in response to the increase in blood pressure. High blood pressure causes the heart rate to decrease, and then the blood pressure decreases. Low blood pressure reduces the activity of the baroreceptor reflex, and as a result, heart rate and blood pressure increase. Our current knowledge of identifying different components of the baroreceptor reflex is the result of numerous preliminary studies that have been carried out on humans and animals. Although the importance of baroreceptors in the control of arterial pressure under resting conditions has never been doubted, there are disagreements about how they function, considering various blood flow rates.

Donald and Edis, in their research on the isolated carotid baroreceptors of dogs, showed for the first time that the baroreflex performance curve undergoes a re-adjustment during exercise compared to the resting state without changing the sensitivity of the baroreceptors [1]. Later studies confirmed this finding in humans and showed that the amount of this re-regulation has a direct relationship with the intensity of exercise. Feng et al. and his colleagues conducted studies on the numerical modeling of aortic arch baroreceptors. They combined finite element modeling with laboratory work on the aortic arch of a rat. Numerical simulation in this study could show the functional role of axial loading in the baroreceptor region of the aortic arch. The laboratory studies that were done on the aortic arch of the mouse confirmed the validity of the numerical simulation [2-6]. Lee et al. proposed the CFD method on several carotid bifurcations and illustrated how the zones interacted with the connection among the geometric construction and flowed fluctuation as oscillatory shear parameters [7]. Also, Dong et al. performed blood flow downstream at the carotid branches, resulting from the downstream arterial impedance [8]. According to the FSI analysis of the aortic wall, the study of Suito et al. is performed on the thoracic aorta of the human vascular system. They constructed the geometry of the aorta based on CT images and concentrated on the connection of the WSS distribution in the centerline [9]. Lantz et al. carried out an FSI model of the human aorta using MRI images. They simulated the impact of arterial wall movement on WSS variation by considering the outcomes related to rigid arterial wall results [10]. In this regard, Crosetto et al. proposed similar mathematical modeling with an identical approach. The boundary conditions applied for the vessel outlets were received results in a one-dimensional simulation [11]. In the current study, a three-dimensional aortic arch model is presented as considering various blood flow rates. The mathematical modeling was considered by the FSI method to reach the hemodynamic forces applied to the arterial vessel wall and results in abnormal stresses. Also, more fluid details were analyzed concerning average peak and mean blood velocities corresponding to the ascending aorta inlet blood flow with respect to the previous literature review. Simulation models of different parts of the carotid vascular system have been presented in recent years [12]. A three-dimensional and accurate mathematical model can help to investigate the baroreflex system's performance accurately. The present study investigated a three-dimensional aortic arch model as the expected maximum stress and deformation locations, considering various blood flow rates.

2 METHOD AND MATERIALS

This research intends to quantitatively study the deformation of the aortic wall by creating an accurate three-dimensional model that considers the properties using the fluid-structure interaction (FSI) method. In order to simulate the arteries of the human body, the real dimensions were determined using Mimics software, which modeled the arteries obtained from the positron emission tomography-computed tomography (PET-CT) imaging method. In order to simulate the arteries of the human body, the real dimensions have been determined using Mimics software from the modeling of the arteries obtained from the positron emission tomography-computed tomography (PET-CT) imaging method. Then, the CT scan was transferred to computational fluid dynamics software for the fluid flow part, as well as finite element software for the solid part; modeling and factors such as stress, strain, and deformation were studied. For numerical simulations, the direct interaction between blood and the solid wall of the vessel is used. Strains and deformations will be desired to calculate the response of the flexible vessel wall. While considering the externally applied loads, the velocity, acceleration, and displacement vectors in the vessel domain, along with the pressure and flow fields, are calculated by solving the Equations of motion in the fluid domain. Also, the blood flow in the vessels of the human body is considered a

Newtonian fluid that obeys the dynamic relationships of fluids with specific density and viscosity. Solving the governing Equations in solid-fluid interaction problems is similar to fluid problems with moving boundaries.

2.1. Governing Equations of The Fluid Region

The governing Equations of blood flow are the mass continuity and momentum conservation Equations. The law of conservation of mass is generally expressed as "Eq. (1)".

$$\frac{\partial \rho}{\partial t} + \frac{\partial (\rho u_i)}{\partial x_i} = 0 \tag{1}$$

In three-dimensional flow **i**= 1,2,3, **ρ** is density, **u** is velocity, and **t** is time. The momentum Equation in its general form for incompressible flow and constant viscosity is given by "Eq. (2)".

$$\rho\left(\frac{\partial u_i}{\partial t} + \frac{\partial (u_i u_j)}{x_j}\right) = -\frac{\partial p}{\partial x_i} + \mu \frac{\partial}{\partial x_i}\left(\frac{\partial u_i}{\partial x_j} + \frac{\partial u_j}{\partial x_i}\right) + \rho f_i \tag{2}$$

In this Equation, f_i is the volumetric force on the fluid flow, which can represent the forces acting on the fluid due to gravity.

2.2. Equations Governing the Solid Region of The Vessel

Solving the solid field in problems that include fluid-structure interaction is the same as solid problems, with the difference that after each step of solving the fluid field and its convergence, the forces acting on the solid must also be updated. In the problems of fluid-structure interaction, the solid medium generally exhibits non-linear behavior. The computational domain in fluid-structure interaction problems with dynamic elastic Equations, which include the momentum Equation and the equilibrium Equation, is described by the momentum "Eq. (3)" and the equilibrium "Eq. (4)".

$$\rho \frac{\partial^2 d}{\partial t^2} = \frac{\partial \sigma_{i,j}}{\partial x_j} + \rho f_i \tag{3}$$

$$\sigma_{i,j} \times n_j = \tau_i^s \tag{4}$$

In these Equations, **ρ** is the density of the solid substance, $\partial^2 d/\partial t^2$ represents the acceleration of the point mass of the solid, **d** is the displacement of the point mass, **σ** is the Cauchy stress tensor, $\boldsymbol{f}$ is the external forces applied at time **t**, τ_i^s is the stresses applied to the external surface at time **t**, and **n** is the normal vector to the surface.

2.3. Fluid-Structure Interaction

In order to achieve more realistic results, the physical conditions governing the problem must be fully considered. In the analysis of problems, considering the interaction of fluid and solid, the effect of flow on the wall and the effect of the deformation of the solid wall on the movement of the fluid is considered. In this type of analysis, two separate models are prepared, and the computational domain is divided into two parts: fluid domain and solid domain. When solving these two domains, they should be coupled together and solved simultaneously. The solid model is based on the Lagrangian system. In the Lagrangian view, the motion of a single particle is followed, and its displacement is unknown. The fluid model alone is always analyzed with the Eulerian coordinate system. For fluid-solid interaction problems, a combination of Eulerian and Lagrangian perspectives should be used, which is known as the arbitrary Lagrangian-Eulerian system (ALE). In fact, the Eulerian point of view is used for fluid domain Equations, the Lagrangian point of view is used for solid Equations, and the ALE point of view is used for common boundaries of solid and fluid. In fluid-structure interaction problems, the stresses and deformations of the solid domain are calculated simultaneously with the flow parameters that are in contact with the solid domain. In other words, the changes in the shape of the solid domain are caused by fluid pressure gradients, and in a similar way, the pressures and velocities in the fluid domain are also dependent on the changes in the shape of the solid domain structure.

2.4. Computational Model-Building Steps

The geometry used in this project is from hospital images in DICOM format, which are taken in two dimensions from the body of a healthy person. After importing in the Mimics software, the complete geometry of the cardiovascular system is imaged by specifying the range of rays irradiated to the patient's body and based on the soft tissue, which includes the cardiovascular system as well as the respiratory system. By adjusting the lower and upper limits of the pixels, the images can be seen. Then, by selecting the geometry of the cardiovascular system, which includes the ventricles, atria, and aorta, as well as blood vessels and pulmonary vessels, it was extracted separately, as shown in "Fig. 1".

2.5. Geometry and Boundary Conditions

Based on the research of Gabe et al. [13], the maximum and minimum average blood velocity in the ascending aorta is $0.66\ cm/s$ and $0.11\ cm/s$. Current studies consider three velocities of $0.66\ cm/s$, $0.385\ cm/s$, and $0.11\ cm/s$ cm/s for blood flow simulation [14]. The blood flow at the velocity of $0.11\ cm/s$ is laminar. However, the blood flow at the velocities of $0.66\ cm/s$ and 0.385 cm/s the blood flow is turbulent. The present study is simulated with the $k-\epsilon$ turbulence model based on the study of James et al. [15]. Based on the assumption of Vinoth et al. [16], boundary condition data related to a relative pressure of $120\ mm\ Hg$ is assumed at all aortic branch outlets. Blood density is 1050 kg/m^3, and its dynamic viscosity is $0.0035\ Ns/m^2$. Based on

Giannakoulas et al.'s study [17], Young's modulus is equal to 4.66 Mpa, Poisson's ratio is 0.45, and a density of 1062 kg/m^3 was considered. For all inlets and outlets, the fixed support boundary condition is applied [18]. The amount of displacement in fixed support boundary conditions is zero.

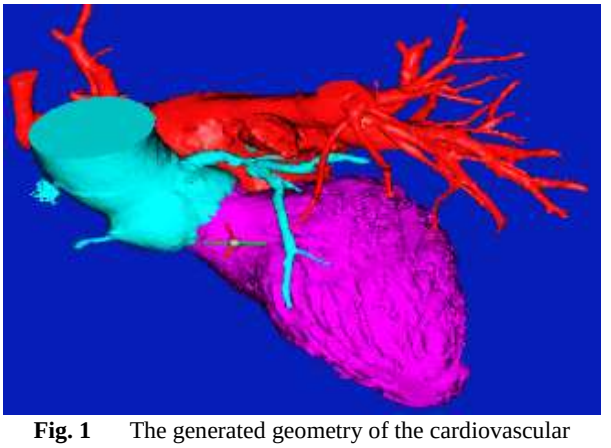

Fig. 1 The generated geometry of the cardiovascular system extracted by Mimics software for a 45-year-old male.

2.6. Mesh Construction

Due to the curved geometry of the blood vessel and its asymmetry during grid generation, it has been tried to use the meshing of tetrahedral elements and boundary layer elements in the vessel wall to achieve more accurate results. The total number of meshes used is selected after checking meshing independence. The grid is made with average Orthogonal Quality=0.78, Skewness=0.21, and Aspect Ratio=1.80 ("Fig. 2").

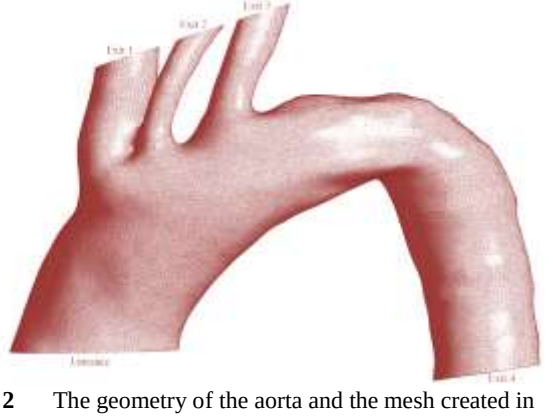

Fig. 2 The geometry of the aorta and the mesh created in the computational model.

In this simulation, the mesh sensitivity analysis was studied. It needs a mesh sensitivity analysis to ensure the problem is independent of the mesh size. In this research, several mesh samples with different sizes and inflation mesh on the vessel walls with a growth rate of 1.2 have been used to achieve better results. Current results considered the amount of equivalent pressure created at the vessel wall as a criterion for the appropriateness of the number of calculation elements, as shown in "Fig. 3".

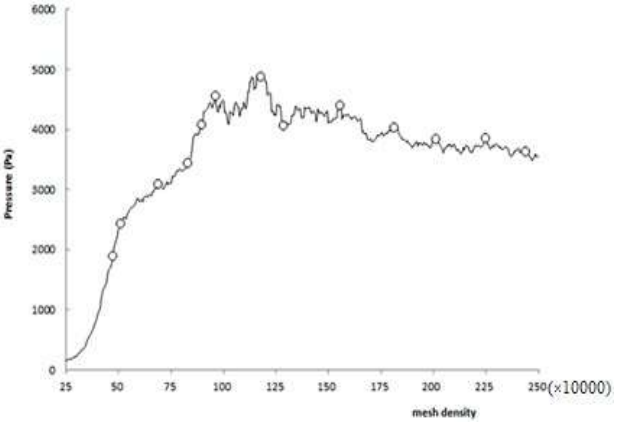

Fig. 3 Mesh sensitivity analysis in the computational model.

The measured maximum and minimum pressure at each location are shown in "Table 1". The measured pressures are relatively low, which is probably due to the patient being anesthetized (part of the standard clinical procedure). The pressure drops, as opposed to the absolute pressure, define the flow through the vessel in the absence of interaction between the fluid and the mechanical properties of the vessel wall; thus, the relatively lower magnitude of the measured pressures would not affect the predicted flow under the present simulation conditions. Table 1 shows that the individual values of Pmax and Pmin at each outlet are within 6% of the pulse pressure. The pulse pressure at each outlet is within 3.5%. In the AA, the maximum pressure is close to the value measured and the mismatch for minimum pressure is 8% of the pulse pressure. Two additional invasive measurements in the distal arch and mid-abdominal aorta (in the TL) were compared with the CFD values for further validation. These were found to be in close agreement as shown in "Table 1" [19].

Table 1 Minimum and maximum pressure values at various locations throughout the domain, measured experimentally and derived from the simulations. The boundaries are labelled: AA–ascending aorta, BT–brachiocephalic trunk, LCC – left common carotid artery, LS–left subclavian artery, DA–descending aorta

	Pressure	AA	BT	LCC	LS	DA
Exp.	P_{min}	56	50	50	N/A	52
	P_{max}	103	97	96	N/A	99
CFD	P_{min}	52.7	52	51.9	52.3	51.1
	P_{max}	103.3	97.9	97.3	97.6	98.1

3 RESULTS AND DISCUSSION

This research used the FSI method based on the leading models obtained from the aorta by real images obtained from PET-CT imaging devices. After running in the Mimics software for modeling based on the actual dimensions and geometry of the vessel, the obtained model is transferred to the Ansys software for analysis and is analyzed in different conditions using the finite volume method. In the present study, blood is considered a Newtonian, incompressible, and isothermal fluid, which is continuous. In simulating the geometry of the aorta, the continuity and Navier-Stokes Equation are the governing Equations for the 3-D blood movement. Also, the boundary condition of the fluid and solid interaction introduces forces from the blood side to the vessel wall. This section draws the pressure and velocity contours for the blood flow domain and the deformation, strain, and stress contours for the vessel's solid domain. These contours are drawn for three blood inflow velocities of 11 cm/s, 38.5 cm/s, and 66 cm/s. Figure 4 shows the static pressure contours in the middle and transverse planes. The maximum amount of pressure occurs in the supra-aorta, reaching 16.04 kPa, 16.41 kPa, and 17.32 kPa at velocities of 11 cm/s, 38.5 cm/s, and 66 cm/s, respectively. Baroreceptors are located at the place of application of this maximum pressure. Also, the lowest pressure occurs in the descending aorta, and the minimum amount at the velocities of 11 cm/s, 38.5 cm/s, and 66 cm/s is 15.98 kPa, 15.84 kPa, and 15.58 kPa, respectively. Therefore, in the descending aorta, the low-pressure area causes blood to be sucked toward the abdominal aorta.

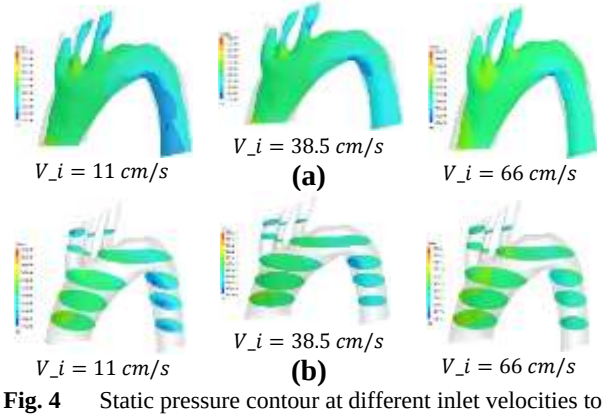

Fig. 4 Static pressure contour at different inlet velocities to the aorta for: (a): middle plane, and (b): transverse planes.

Figure 5 shows the instantaneous velocity contours in the middle and transverse planes. The highest instantaneous velocity occurs in the supra-aorta, and these amounts in inlet velocities of 11 cm/s, 38.5 cm/s, and 66 cm/s reach 0.31 m/s, 1 m/s, and 1.7 m/s, respectively. Also, the lowest instantaneous velocity occurs in the internal arch of the ascending aorta and the internal arch of the descending aorta, so the instantaneous velocity reaches zero at some points.

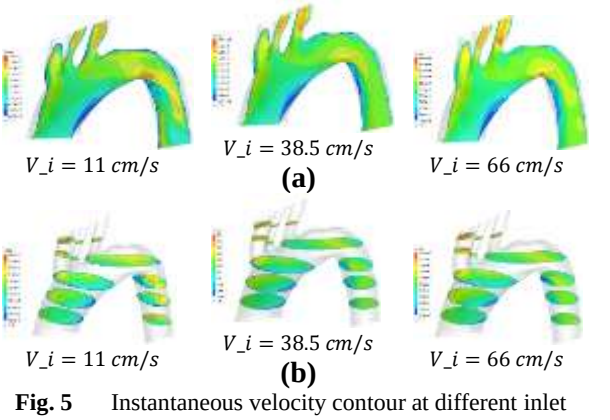

Fig. 5 Instantaneous velocity contour at different inlet velocities to the aorta for: (a): middle plane, and (b): transverse planes.

Figure 6 presents the contours of normal stress and wall strain. The highest normal stress occurs in the posterior supra aorta. So, the amount of this maximum vertical stress increases up to 5 kPa in some places; these points have higher tensions and can be susceptible to rupture and aneurysm diseases. This could be an area of potential aneurysm development based on clinical evidence of rupture locations. Also, the highest strain occurs in the posterior supra aorta, reaching 0.001. Figures 6a and 6b show almost the same distributions because of the direct relation between stress and wall strain alteration.

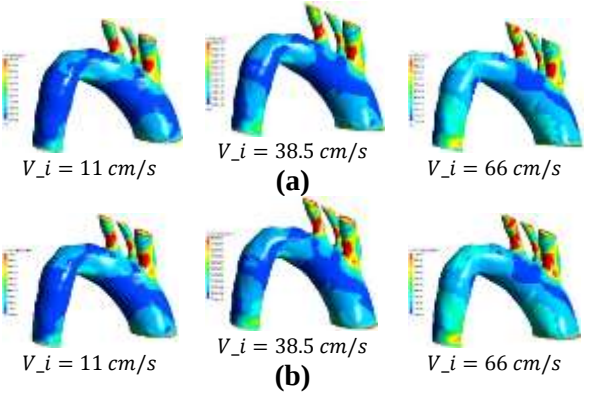

Fig. 6 Normal stress and wall strain contours at different inlet velocities to the aorta for: (a): normal stress, and (b): wall strain.

Baroreceptors are usually located in the adventitia layer of the aortic arch. Aging is usually accompanied by a hardening of the arterial walls or atherosclerosis, which leads to a decrease in the ability of blood pressure receptors to heart rate and control blood pressure [20-21]. Therefore, the factor that determines the location of baroreceptors can be the maximum normal stress, which

can be calculated by solving the problem in the form of fluid and structure interaction in the vessel wall. Hence, the value of Young's coefficient of the vessel wall plays a key role in determining the location of baroreceptors.

4 CONCLUSIONS

This research investigates the blood flow and wall shape changes in the aorta during different blood flow rates as much as possible. Steady flow with a Newtonian fluid in a realistic aorta geometry was investigated. This enables us to investigate more complex boundary conditions in the future than what is used in this research. It has also been tried to better understand flow physics by producing suitable results. In this regard, various flow parameters, such as blood velocity, blood pressure, stress, and strain on the vessel wall, were investigated from different views. The results show that the highest vertical stress occurs in the posterior supra aorta. So, the amount of this maximum vertical stress increases up to 5 kPa in some places; these points have higher tensions, and they can be susceptible to rupture and aneurysm diseases.

REFERENCES

[1] Donald, D. E., Edis, A. J., Comparison of Aortic and Carotid Baroreflexes in the dog, J. Physiol, Vol. 215, No. 2 1971, pp. 521-38, Doi: 10.1113/jphysiol. 1971.sp009483.

[2] Feng, B., Li, B. Y., Nauman, E. A., and Schild, J. H., Theoretical and Electrophysiological Evidence for Axial Loading About Aortic Baroreceptor Nerve Terminals in Rats, Am J Physiol Heart Circ Physiol, Vol. 293, No. 6, 2007, pp. 3659-72.

[3] Carlson, B. E., Arciero, J. C., and Secomb, T. W. Theoretical Model of Blood Flow Autoregulation: Roles of Myogenic, Shear-Dependent, And Metabolic Responses, American Journal of Physiology-Heart and Circulatory Physiology, Vol. 295, No. 4, 2008, pp. 1572-1579,

[4] Rizzo, D. C., Fundamentals of Anatomy and Physiology, Cengage Learning, 2015.

[5] Bisognano, J., Sloand, J., Papademetriou, V., Rothstein, M., Sica, D., Flack, J., and Cody, R. J., An Implantable Carotid Sinus Baroreflex Activating System for Drug-Resistant Hypertension: Interim Chronic Efficacy Results from The Multi-Center Rheos Feasibility Trial, 2006.

[6] Kroon, A., Schmidli, J., Scheffers, I., Tordoir, J., Mohaupt, M., Allemann, and De Leeuw, P., Sustained Blood Pressure Reduction by Baroreflex Activation Therapy with A Chronically Implanted System: 4-Year Data of Rheos Debut-Ht Study in Patients with Resistant Hypertension: 9D. 01, Journal of Hypertension, Vol. 28, No. 441, 2010.

[7] Lee, S. W., Antiga, L., Spence, J. D., and Steinman, D. A., Geometry of the Carotid Bifurcation Predicts Its Exposure to Disturbed Flow, Stroke Vol. 39, No. 8, 2008, pp. 2341–7.

[8] Dong, J., Wong, K. K. L., and Tu, J., Hemodynamics Analysis of Patient- Specific Carotid Bifurcation: a CFD Model of Downstream Peripheral Vascular Impedance, Int J Numer Method Biomed Eng, Vol. 29, No. 4, 2023, pp. 476–91.

[9] Suito, H., Takizawa, K., Huynh, V. Q. H., Sze, D., and Ueda, T., FSI Analysis of The Blood Flow and Geometrical Characteristics in The Thoracic Aorta, Comput Mech, Vol. 54, No. 4, 2022, pp. 1035–45.

[10] Lantz, J., Renner, J., and Karlsson, M., Wall Shear Stress in A Subject Specific Human Aorta—Influence of Fluid-Structure Interaction. Int. J. Appl Mech, Vol. 3, No. 04, 2021, pp. 759–78.

[11] Crosetto, P., Reymond, P., Deparis, S., Kontaxakis, D., Stergiopulos, N., and Quarteroni, A., Fluid–Structure Interaction Simulation of Aortic Blood Flow. Comput Fluids, Vol. 43, No. 1, 2021, pp. 46–57.

[12] Klabunde, R., Cardiovascular Physiology Concepts, Lippincott Williams & Wilkins, 2011.

[13] Kougias, P., Weakley, S. M., Yao, Q., Lin, P. H., and Chen, C., Arterial Baroreceptors in The Management of Systemic Hypertension, Med Sci Monit Int Med J Exp Clin Res, Vol. 16, No. 1, RA1, 2010.

[14] Gabe, I. T., Gault, J. H., Ross, J. Jr., Mason, D. T., Mills, C. J., Schillingford, J. P., and Braunwald, E., Measurement of Instantaneous Blood Flow Velocity and Pressure in Conscious Man with A Catheter-Tip Velocity Probe, Circulation, Vol. 40, No. 5, 1969, pp. 603-14.

[15] James, M. E., Papavassiliou, D.V., and O'Rear, E. A., Use of Computational Fluid Dynamics to Analyze Blood Flow, Hemolysis and Sublethal Damage to Red Blood Cells in a Bileaflet Artificial Heart Valve, Fluids, Vol. 4, No. 19. 2019, https://doi.org/10.3390/fluids4010019.

[16] Vinoth, R., Kumar, D., Raviraj, A., and Vijay Shankar C. S., Non-Newtonian and Newtonian blood flow in human aorta: A transient analysis, Biomedical Research (India), Vol. 28, 2016.

[17] Giannakoulas, G., Giannoglou, G., Soulis, J., Farmakis, T., Papadopoulou, S., Parcharidis, G., and Louridas, G., A Computational Model to Predict Aortic Wall Stresses in Patients with Systolic Arterial Hypertension, Med Hypotheses, Vol. 65, No. 6, 2005, pp. 1191-5, Doi: 10.1016/j.mehy.2005.06.017. Epub 2005 Aug 16. PMID: 16107302.

[18] Kass, J. S., Mizrahi, E. M., Neurology Secrets E-Book. Elsevier Health Sciences, 2016.

[19] Heesch, C. M, Reflexes that Control Cardiovascular Function, Adv Physiol Edu, Vol. 277, No. 6, 1999, pp. 234.

[20] Klabunde, R., Cardiovascular Physiology Concepts, Lippincott Williams & Wilkins, 2011, pp. RA1–8.

[21] Kougias, P., Weakley, S. M., Yao, Q., Lin, P. H., and Chen, C., Arterial Baroreceptors in The Management of Systemic Hypertension, Med Sci Monit Int Med J Exp Clin Res, Vol. 16, No. 1, 2010, RA1.